Dyes and Pigments 214 (2023) 111197

Contents lists available at ScienceDirect

Dyes and Pigments

journal homepage: www.elsevier.com/locate/dyepig

Design of donor-acceptor small molecules based on diazaisoindigo unit: Synthesis, theoretical calculations and photophysical studies

M. Belén Martin [a], Álvaro Recuero [a], Andrés Garzón-Ruiz [b], Mónica Moral [c], Gonzalo García-Espejo [d], Juan Cabanillas-Gonzalez [e], Gustavo de Miguel [d,**], Eva M. García-Frutos [a,f,*]

[a] Instituto de Ciencia de Materiales de Madrid (ICMM), CSIC, Cantoblanco, Madrid, 28049, Spain
[b] Departamento de Química Física, Facultad de Farmacia, Universidad de Castilla-La Mancha, C/ José María Sánchez Ibáñez s/n, 02071, Albacete, Spain
[c] Facultad de Educación, Universidad de Castilla-La Mancha, Campus Universitario s/n, 02071, Albacete, Spain
[d] Departamento de Química Física y Termodinámica Aplicada, Instituto Químico para la Energía y el Medioambiente (IQUEMA), Universidad de Córdoba, Campus de Rabanales, Edificio Marie Curie, 14071, Córdoba, Spain
[e] Madrid Institute for Advanced Studies, IMDEA Nanoscience, Calle Faraday 9, 28049, Madrid, Spain
[f] Facultad de Farmacia, Universidad de Alcalá, Campus Universitario. Ctra. Madrid-Barcelona Km.33,600, 28871, Alcalá de Henares, Madrid, Spain

ARTICLE INFO

Keywords:
π-conjugated materials
Electron-acceptor
7,7′-diazaisoindigo derivatives
Organic electronics
Photophysics
Transient absorption spectroscopy

ABSTRACT

Two donor-acceptor-donor (D–A–D) and two donor-acceptor (D-A) small molecular systems involving alkyl bithiophene and thiophene derivatives as donor blocks and 5,5′- and 5-linked 7,7′-diazaisoindigo (DAIID) as acceptor blocks have been synthesized and investigated with theoretical calculations and photophysical studies. The incorporation of the thiophene groups led to significant changes in the UV–vis absorption spectra and electronic structure of the diazaisoindigo. Bithiophene and thiophene derivatives did not show fluorescence, in contrast to their dibrominated and brominated precursors. This fact was attributed to both a decrease of the radiative rate constant and an increase of the non-radiative deactivation associated to the incorporation of the thiophenyl groups. Additionally, picosecond transient absorption experiments revealed short time decays for the thiophenyl derivatives indicating a faster non-radiative deactivation associated to a rotation of the central double bond of 7,7′-diazaisoindigo in the excited state.

1. Introduction

Organic π-conjugated pigments have attracted great attention as semiconducting materials for organics electronics applications, such as organic field effect transistors (OFETs), organic light emitting diodes (OLEDs), organic solar cells (OSCs), and photodetectors [1–5]. A huge amount of studies about organic semiconductors have been reported, depicting the ease of synthesis, stability, low-cost, light-weight, and mechanical flexibility, as well as versatility, considering the advantages of tuning the optical and electronic properties by changing the chemical design. During the past few years, many classes of organic π-conjugated polymers and molecules, based on donor–acceptor (D–A) moieties, have been developed for organic electronics applications [6,7]. Well-defined small organic molecules show benefits compared to conjugated polymers, such as larger reproducibility of the synthesis, easier purification process, well-defined chemical structure, and monodispersed molecular weight. The strategy of alternating D–A conjugation in the small molecules has afforded a huge amount of organic semiconductors with excellent performances in organic optoelectronic devices [8]. These D-A small molecules, or push-pull systems, entail an intramolecular charge transfer, which is useful for widening the absorption spectrum and reduce the optical band gap [9]. In the D-A systems, the most widely used donor units (p-type organic compounds) are thiophene-based systems, while a wide range of organic structures have been employed as the electron acceptors units (n-type organic compounds) [10]. Among the employed acceptor units for organic electronics, it is worthy remarking moieties such as benzothiadiazole [11,12], diketopyrrolopyrrole (DPP) [13–15], imide and amide-based units

* Corresponding author. Facultad de Farmacia, Universidad de Alcalá, Campus Universitario. Ctra. Madrid-Barcelona Km.33,600, 28871, Alcalá de Henares, Madrid, Spain.
** Corresponding author.
E-mail addresses: q62mirog@uco.es (G. de Miguel), emgfrutos@icmm.csic.es (E.M. García-Frutos).

https://doi.org/10.1016/j.dyepig.2023.111197
Received 13 September 2022; Received in revised form 22 December 2022; Accepted 27 February 2023
Available online 28 February 2023

[2], and isoindigo and derivatives [16–20].

Isoindigo is a structural isomer of the well-known natural pigment indigo that can be found in plants such as isatis tinctoria [21]. Chemically, isoindigo [22] possesses acceptor unit properties, as it is formed by an electron-deficient symmetrical benzene-fused five-membered lactam rings, connected through an exocyclic double bond placed at the 3 and 3′ positions, giving rise to a completely conjugated systems. From 2010 [23], when isoindigo was described as an ideal acceptor unit in D-A small molecules in organic solar cells and field effect transistors, many different isoindigo-based structures and derivatives have been described, with the goal of boosting device performance [22,24–27]. In fact, other new derivatives of isoindigo, such as the diazaisoindigo, have attracted great attention to achieve this goal, as, for example, the non-functionalized *N,N*-dialkyl diazaisoindigo [28]. In the diazaisoindigo (DAIID) molecule, two C atoms have been replaced by two N atoms in the benzene fused to the electron-deficient symmetrical lactam core. These two sp^2-nitrogen atoms can be located at different positions in the benzene ring. Several DAIID have been described, such as 7-DAIID [28–31] and 5-DAIID [32], where the N atoms are placed at different positions, affording a strong effect on their photophysical properties changing the LUMO level. Additionally, the diazaisoindigo unit can have two possible linkages (5,5′- vs 6,6'-) to design and develop versatile and new D-A and D-A-D materials as acceptor units [33–36]. In the last years, some studies on the conventional 6,6′-linked diazaisoindigo, prepared via the Suzuki coupling, have been reported as D-A semiconductors. However, the 5,5′-linked diazaisoindigo has been much less studied.

Herein, we have designed a family of D-A and D-A-D compounds bearing diazaisoindigo (DAIID) as a central acceptor moiety connected at the 5 or 5,5' positions and alkyl-substituted thiophenes or bithiophenes as donors in order to tune the HOMO-LUMO gap. Density functional calculations and transient absorption spectroscopy studies are deployed to shed light into the effect of donor and alkyl substitution position on molecular conformation, absorption spectra and excited-state dynamics of the resulting dyads and tryads

2. Experimental section

2.1. General

All reagents for the synthesis of products were purchased from Merck/Sigma-Aldrich. Solvents were purchased from Scharlab. All reactions were monitored by silica gel thin layer chromatography using a UV light (254 nm). Column chromatography was carried out on silica gel (200–300 mesh). ^{1}H and ^{13}C NMR spectra were obtained on a Bruker AVANCE 300/200 spectrometer, 300 and 200 MHz (^{1}H) or at 75.4 and 50 MHz (^{13}C) at 25 °C, in 5 mm tubes at room temperature with $CDCl_3$ as the solvent. Chemical shifts (δ) are quoted in parts per million (ppm), referenced to residual solvent. Mass spectra were confirmed using Matrix Assisted Laser Desorption (MALDI) mass spectrometer in positive ion reflector mode.

2.2. Spectroscopy experiments

UV–visible absorption spectra were measured on a Cary 100 Bio UV–visible spectrophotometer. Steady-state and time-resolved fluorescence measurements were performed on FLS920 Fluorimeter (Edinburgh Instrument Ltd, Livingston, UK). The transient spectroscopy set-up consisted of a femtosecond Clark MXR regenerative amplifier as primary source delivering 120 fs pulses at 775 nm and 1 KHz repetition rate. The primary beam was split into two. One part was frequency doubled to 387 nm in a β-BaB_2O_4 (BBO) crystal and used as the pump beam. Subsequently, it was sent into a computer controlled delay line before being focused onto the sample to yield 10 μJ cm^{-2} excitation energy flux. The other beam was in turn focused into a sapphire plate to generate a super continuum probe and was spatially overlapped with the pump spot on the sample. A spectrometer equipped with a double array optical multichannel detector (Entwicklungsbuero Stresing) operating in single shot acquisition mode was employed to monitor both the transmitted light through the sample and a split-off fraction of the probe as reference. Using a reference channel allows us to record the absorption spectrum for each laser shot, thus monitoring the differences in absorbance upon two consecutive pump-on pump-off acquisitions. This approach reduces to half the number of laser pump shots to which the sample is exposed.

2.3. Computational details

All the calculations were performed with the Gaussian16 (revision C.01) suite of programs [37]. The ground state geometry of compounds **1**, **2**, **3**, **5**, **6**, **7** and **8** was optimized using the PBE0 functional [38,39] together with the 6-31G** basis set. Polarizable Continuum Model (PCM) methodology was employed to include solvent effects (toluene solvent) [40,41]. Vertical electronic transitions were computed at the time-dependent density functional theory level (TD-PBE0/6-31G*) including solvent effects [40,41]. The intramolecular charge transfer (ICT) character of the electronic transitions was evaluated trough the Δr index, a parameter proposed by Adamo and coworkers to measure charge transfer length during electron excitation [42]. Δr index was calculated employing the Multiwfn 3.8 code [43].

3. Results and discussion

The general synthetic route of the target molecules is depicted in Scheme 1 and S1. The synthesis by an aldol condensation between 5-bromo-7-azaisatin and 7-azaindolin-2-one affords a crude of a mixture of three diazaisoindigos (DAIID) with different substitutions (R = R' = Br, R = H R' = Br and R = R' = H), as illustrated in Scheme S1, analogously to the method described in the literature [44]. These mixture of three diazaisoindigos is inseparable due to the poor solubility of the platform. The incorporation of the alkyl groups at the nitrogen position enables solution processing of the DAIID. This *N*-alkylation was carried out with 1-iodododecane in the presence of K_2CO_3 as a base in DMF at 100 °C during 2 h. The crude was purified *via* flash chromatography to afford isolation of 7,7′-DAIID-Br_2 (**1**) [29], 7,7′-DAIID-Br (**2**), and 7,7′-DAIID (**3**) separately (Scheme S1). Finally, the incorporation of the thiophene group to afford the final donor–acceptor–donor (D–A–D) (**5**, **6**) (Scheme 1a) and donor–acceptor (D–A) (**7**,**8**) (Scheme 1b) 7,7′-DAIID has been effectively prepared by using the typical Suzuki coupling conditions from 7,7′-DAIID-Br_2 (**1**) and 7,7′-DAIID-Br (**2**) compounds, respectively.

Chemical structures of the intermediates and final compounds were confirmed by ^{1}H and ^{13}C nuclear magnetic resonance (NMR) spectra, high resolution matrix-assisted laser desorption/ionization time-of-flight (MALDI-TOF) mass spectra, and exact mass (See Supporting Information for full details on synthesis and spectroscopic characterization).

Theoretical calculations were performed to investigate potential changes in molecular geometry and energies of the HOMO-LUMO orbitals upon the thiophenyl substitution. The ground state molecular geometry was calculated for **1** and **2** (di- and mono-bromine reference molecules), **5** and **6** (di-thiophenyl derivatives) and **7** and **8** (mono-thiophenyl derivatives) at the PBE0/6-31G* level of theory including solvation effects (toluene) (see some examples in Fig. 1 and S1). The insertion of bromine in the 5 or 5,5′ positions of the diazaisoindigo platform (**1** and **2** molecules) does not produce any change in the planarity of the platform with respect to the unsubstituted 7,7′-diazaisoindigo (0.0°) while the **7** and **8** derivatives are slightly twisted with a dihedral angle between the two aza-oxindole moieties of 6.2° and 6.3°, respectively (see Fig. 1A) [28,30]. Regarding the **5** and **6** derivatives, the calculated dihedral angles are 0.4°. The rather small values for the dihedral angles that determine the planarity of the molecule might be

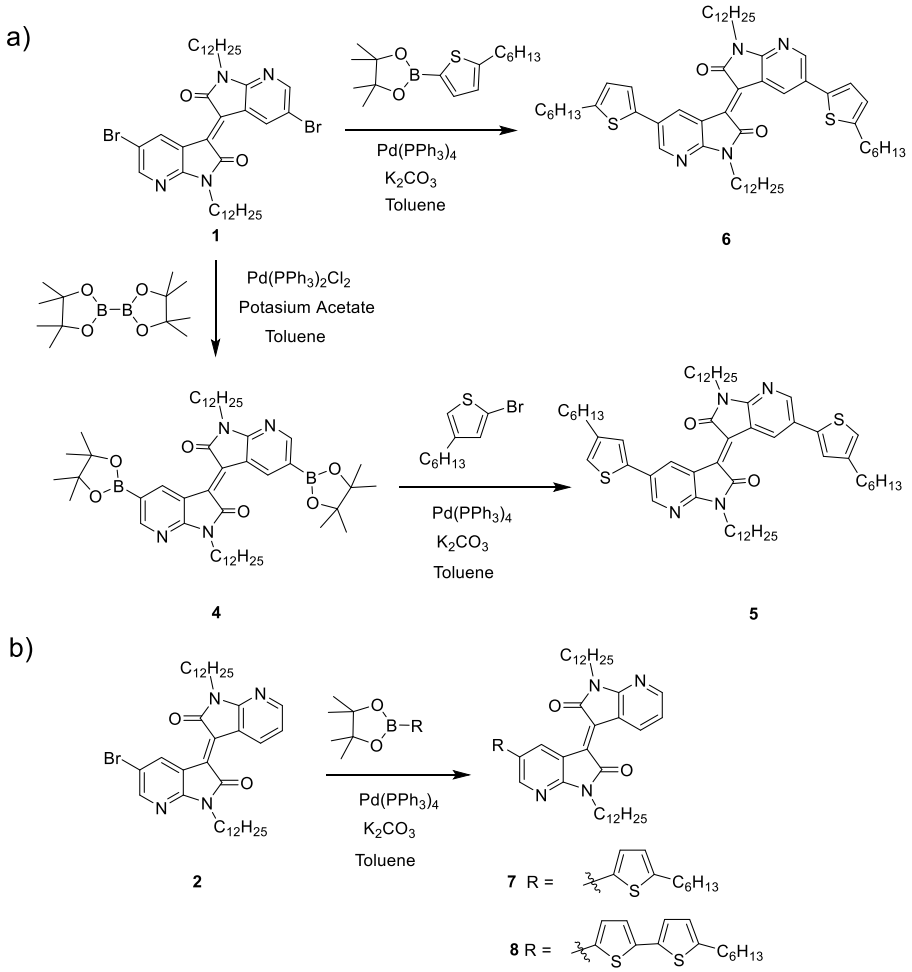

Scheme 1. a) Synthetic route of the 7,7′-DAIID derivatives **5**, **6**; b) synthetic route of the 7,7′-DAIID derivatives **7**, **8** under Suzuki coupling conditions.

governed by the short distance between the O atom of the carbonyl groups and the H atom bound to the C atom at position 4 of each aza-oxindole moiety, between 1.97 and 1.98 Å for compounds **1**, **2**, **5** and **6**, smaller than the sum of their van der Waals radii [45]. This finding suggests that the formation of two intramolecular H-bonds must favor the planar structure of the 7,7′-diazaisoindigo core. The loss of planarity observed in mono-substituted compounds **7** and **8** could be explained due to a slightly larger O···H distances (1.99–2.00 Å). The incorporation of the thiophenyl groups to the diazaisoindigo platform has significant effects on the electronic structure. It is observed a change in the localization of the HOMO and LUMO orbitals in the **5**–**8** derivatives, as well as an energy increase, especially the HOMO orbital, with respect to **1** and **2** accompanied by a reduced HOMO-LUMO gap (2.81 eV in **5**, 2.75 eV in **6**, 2.79 eV in **7** and 2.45 eV **8** in contrast with 3.16 eV in **1** or 3.24 eV in **2**).

Fig. 2 displays the normalized UV–vis absorption spectra in toluene along with the oscillator strengths of the vertical electronic transitions computed for compounds **1**, **2**, **5**, **6**, **7** and **8** at the TD-PBE0/6-31G* level of theory (including PCM solvation). Table 1 shows the absorption maximum wavelengths (λ_{ab}^{max}) as well as the wavelengths computed for the most relevant vertical electronic transitions (λ_{vert}^{calc}). The absorption spectra of **1** and **2** include three absorption peaks centered around 290, 335 and 500 nm, comparable to those observed in the non-functionalized *N,N*-dialkyl diazaisoindigo **9**, **10** and **11** derivatives (Scheme S2) but shifted to lower energies [28]. As reported for a related molecule, the lowest energy band is weak and corresponds to a HOMO→LUMO transition [30]. The bands centered at about 335 nm are ascribed to HOMO-2→LUMO transitions while the bands centered around 290 nm are associated to electronic transitions involving multiple contributions. The charge transfer length (Δr) is very small for all the most relevant electronic transitions of **1** (Δr ≤ 0.010 Å) suggesting that all of them correspond to local state (LE) transitions. The assessment of the frontier molecular orbitals shows that Br atoms do not have a significant contribution to the virtual orbitals but participate in the occupied orbitals. Nevertheless, the symmetrical structure of **1** (*quasi*-C_{2h}) suggests that the charge transfers from Br atoms to the 7,7′-diazaisoindigo does not lead to a significant separation between the electron and hole centroids. On the contrary, the non-symmetrical structure of the mono-brominated **2** derivative leads to a large increment in the value of Δr (0.5–1.8 Å). The intramolecular charge transfer (ICT) character is predicted to be greater for the band centered at 287 nm in **2**.

Regarding the **5** and **6** di-substituted derivatives, both spectra are identical revealing the limited influence of the position of the hexyl substitution on the optical transitions. Both spectra depict three absorption features located at 320, 380 and 550 nm, red-shifted compared to the brominated derivatives. Interestingly, the bands at 550 nm are weaker than the lowest energy absorption bands recorded for **1** and **2**. Accordingly, the predicted oscillator strength for the HOMO→LUMO transition of **5** and **6** is smaller than that for the same transition in **1** and **2**. The HOMO orbital is delocalized on the whole π-conjugated system while LUMO orbital is located on the 7,7′-diazaisoindigo core (Fig. 1B). Thus, the charge transference from the thiophene rings to the 7,7′-diazaisoindigo core results in an insignificant charge transfer length (Δr ≤ 0.001 Å) suggesting the absence of separation between the electron and hole centroids.

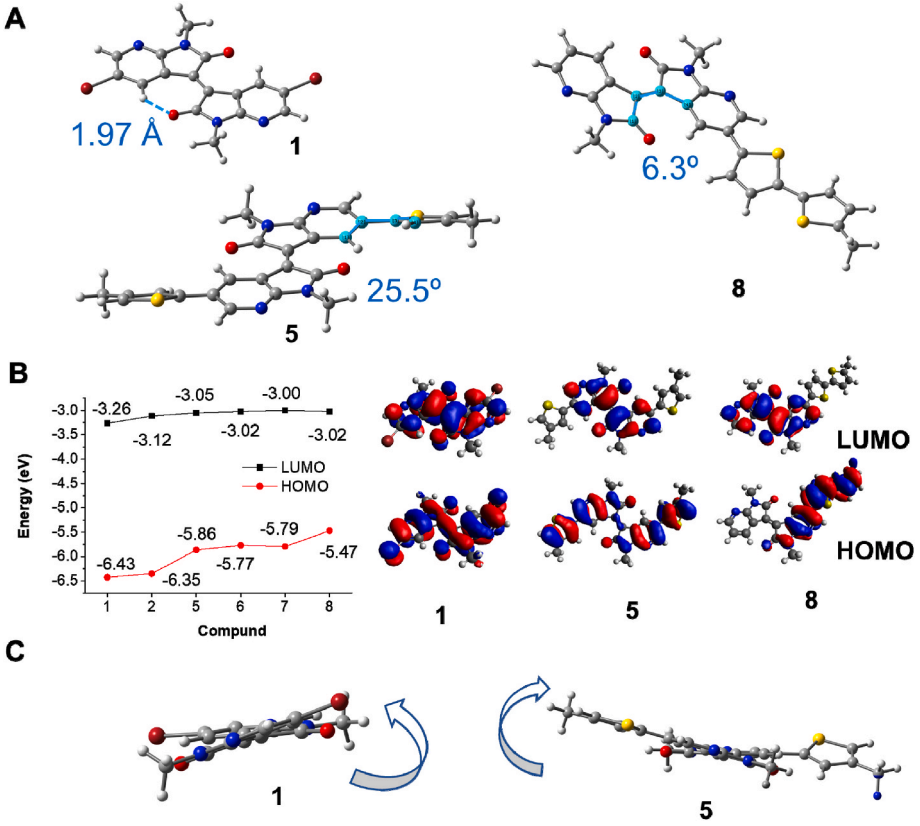

Fig. 1. (A) Optimized ground state molecular geometries at the PBE0/6-31G* level of theory including PCM solvation (toluene). Some relevant molecular parameters (intramolecular distances and dihedral angles) are shown. (B) Energy and shape of HOMO and LUMO orbitals calculated for **1**, **5** and **8**. (C) Optimized excited S_1 state molecular geometries for **1** and **5** at the TD-PBE0/6-31G* level of theory including PCM solvation.

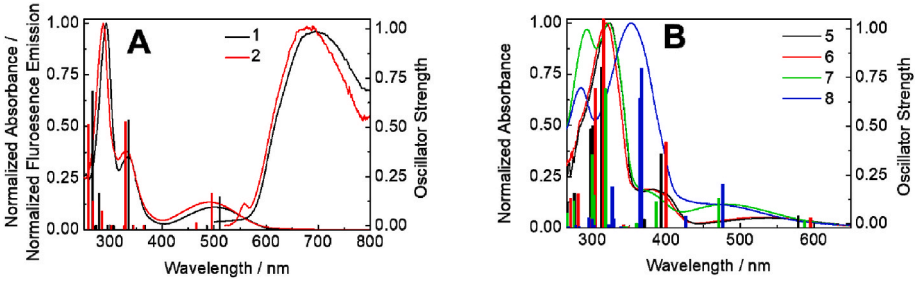

Fig. 2. Normalized absorbance spectra of **1** and **2** (A) and **5**, **6**, **7** and **8** (B) in toluene solution. Fluorescence emission spectra of **1** and **2** (λ_{exc} = 475 nm) are also included in (A). Vertical bars correspond to the oscillator strength (*f*) computed for the electronic transitions at the PBE0/6-31G* level of theory (including PCM solvent).

In case of the mono-substituted derivatives, **7** and **8**, the absorption spectra also reveal the presence of three peaks but with a slightly different arrangement. Thus, both spectra exhibit peaks around 290 and 480 nm, with an additional peak around 320 nm and 350 nm for **7** and **8**, respectively. TD-DFT calculations predicted that the HOMO→LUMO transition is extremely weak (f = 0.003 and 0.001 for **7** and **8**, respectively) not being experimentally observed. Therefore, the lowest energy band is associated to a HOMO-1→LUMO transition for both compounds (λ_{ab}^{max} = 480 nm) appearing blue-shifted with respect to the absorption bands of **1**, **2**, **5** and **6** attributed to the HOMO→LUMO transition (λ_{ab}^{max} = 500–550 nm). Both HOMO-1 and LUMO are mainly located on the 7,7′-diazaisoindigo core with a minor contribution of the thiophene rings in the HOMO-1 orbital. On the contrary, the HOMO→LUMO+1 mainly occurs on the thiophene groups (and their linked aza-oxindole moiety). This electronic transition was associated to the high energy absorption band observed for **7** at around 292 nm. This band is red-shifted up to 352 nm in **8** due to the extension of the π-conjugation in the bi-thiophenyl group. In general, the highest charge transfer lengths were computed for compounds **7** and **8** (Δr = 0.4–2.5 Å).

Fig. 2A also shows the fluorescence emission spectra of **1** and **2**, a broad band peaking at 700 nm and red-shifted compared to the non-functionalized *N,N*-dialkyl diazaisoindigo **9**, **10** and **11** derivatives. Regarding the rest of the substituted derivatives, they did not exhibit any photoluminescence in line with the low photoluminescence quantum yields characteristic of many isoindigos [46]. In general, the weak fluorescence observed in 7,7′-diazaisoindigos is attributed to the rotation around the central double bond upon excitation. This change in the molecular structure allows to reach a conical intersection point between S_1 and S_0 states [28,30]. In this sense, dihedral angles between 12° and 18° have been computed in the S_1 state for all the studied compounds. To account for the absence of fluorescence signal in **5**–**8**, a decrease in the radiative rate (k_r) constant in **5**–**8** compared to **1**–**2** could be considered.

Table 1
Experimental maximum absorption wavelength (λ_{ab}^{max}) (toluene solution). Wavelengths calculated for the most relevant vertical electronic transitions (λ_{vert}^{calc}) calculated at the TD-PBE0/6-31G* level of theory along with the oscillator strengths (*f*) and orbital contribution. Δr related to the charge transfer length.

Comp.	λ_{ab}^{max} (nm)	λ_{vert}^{calc} (nm)	*f*	Transition	Main component of the transition (≥20% contribution)	Δr (Å)
1	500	510	0.15	$S_0 \rightarrow S_1$	H→L(98)	0.002
	335	336	0.54	$S_0 \rightarrow S_5$	H-2→L(98)	0.001
	292	266	0.68	$S_0 \rightarrow S_{13}$	H→L+1(79)	0.010
2	491	495	0.16	$S_0 \rightarrow S_1$	H→L(98)	0.853
	332	329	0.53	$S_0 \rightarrow S_5$	H-2→L(97)	0.536
	287	258	0.51	$S_0 \rightarrow S_{11}$	H-9→L(30); H→L+2 (26); H→L+1(21)	1.764
5	550[a]	579	0.06	$S_0 \rightarrow S_1$	H→L(99)	0.001
	382	393	0.36	$S_0 \rightarrow S_3$	H-2→L(94)	0.001
	323	312	0.78	$S_0 \rightarrow S_{10}$	H-6→L(64)	0.003
6	550[a]	595	0.05	$S_0 \rightarrow S_1$	H→L(99)	0.001
	378	399	0.42	$S_0 \rightarrow S_3$	H-2→L(98)	0.001
	319	315	1.18	$S_0 \rightarrow S_{10}$	H-6→L(65)	0.005
7	481	471	0.14	$S_0 \rightarrow S_2$	H-1→L(93)	1.524
	~380[b]	386	0.13	$S_0 \rightarrow S_3$	H-2→L(83)	1.971
	322	318	0.68	$S_0 \rightarrow S_8$	H-4→L(66); H-7→L (20)	1.089
	292	300	0.36	$S_0 \rightarrow S_{10}$	H→L+1(62); H-8→L (20)	0.428
8	480	476	0.21	$S_0 \rightarrow S_2$	H-1→L(88)	0.954
	352	366	0.78	$S_0 \rightarrow S_4$	H→L+1(46); H-8→L (24)	1.040
		365	0.63	$S_0 \rightarrow S_5$	H→L+1(48); H-8→L (27)	0.920
	295	327	0.20	$S_0 \rightarrow S_9$	H-5→L(39); H-6→L (27)	2.528

[a] Very weak band.
[b] Shoulder.

Thus, the Strickler–Berg relation establishes that k_r is directly related to the oscillator strength, *f* [47,48]. The value of *f* significantly decreases for the $S_0 \rightarrow S_1$ transition in the thiophene substituted derivatives (for instance, *f* is 0.15 for **1**, 0.06 for **5** and 0.003 for **7**). Therefore, a lower k_r should be expected for **5**–**8** with respect to **1** and **2**. Similar results were reported for a series of isoindigo derivatives in which phenyl, thienyl and 3,4-ethylenedioxythien-2-yl groups are attached to the same position that the thienyl groups of **5** and **6** derivatives [46].

The dependence of the fluorescence emission spectrum with the solvent polarity was studied for compounds **1** and **2**. The solubility of these compounds is high in non-polar solvents but very low in polar solvents so that we have only used CCl_4, toluene, anisole, $CHCl_3$ and CH_2Cl_2 in the solvent polarity measurements. We observed a slight red-shift of the maximum of the fluorescence peak when increasing the dielectric constant of the solvent (Fig. S2). The linear relationship is quite good for all solvents except for CCl_4 which may be attributed to a specific effect in this solvent. As expected, a higher slope was found for the Lippert-Mataga plot of **2** (2.78×10^3 cm^{-1}) than for **1** (1.44×10^3 cm^{-1}). Accordingly, the largest change in the dipole moment upon the excitation (μ_E-μ_G) was calculated for compound **2** (4.4 D for **1** and 5.8 D for **2**, considering an effective radius of Onsager cavity of 5.17 and 4.98 Å for **1** and **2**, respectively). The change in the dipole moment obtained for both **1** and **2** is small in comparison with the μ_E-μ_G values typically reported for ICT compounds such as 1,3,5-tristyryl-*s*-triazine (27.8 D) [49], 1,3,5-tristyrylbenzene (14.1 D) [49] and its carbazole and triphenylamine derivatives (14.1–21.1 D) [50], 4-styryl-1,8-naphthalimides (20.8–23.0 D) [51], and boradiazaindacenes (12.2–12.7 D) [52], among others.

To shed light into the excited state de-activation of the studied molecules, femtosecond transient absorption (TA) experiments were performed upon excitation at 387 nm. Fig. 3A displays the TA spectra of **1** in toluene at different time delays. The initial spectrum at 1.3 ps after the photoexcitation shows a positive broad band centered around 550 nm being ascribed to excited state absorption (ESA). At increasing time delays, the intensity of the transient feature decreases and almost vanishes at 65 ps delay. The TA experiments were also performed in $CHCl_3$ and CH_2Cl_2 to investigate the influence of the solvent polarity on the photophysics. There is no change in the shape of the transient spectra in these solvents, but the kinetics are largely affected. Fig. 3B exhibits the decay of the ESA for **1** (λ_{probe} = 550 nm) displaying an acceleration of the TA dynamics upon increasing the solvent polarity. The solvent dependence of the TA signals is in good agreement with that observed for the non-functionalized *N,N*-dialkyl diazaisoindigo **9**, **10** and **11** derivatives proving that the de-activation of the excited state of **1** should follow the same mechanism: a non-radiative internal conversion process via a conical intersection which involves rearrangement of bonds together with intramolecular electron transfer reactions [28,53].

The time profiles are fitted using mono-exponential functions giving time constants of 53, 21 and 12 ps in toluene, $CHCl_3$ and CH_2Cl_2, respectively. These values resemble well the fluorescence lifetimes obtained for the non-functionalized *N,N*-dialkyl diazaisoindigo **9**, **10** and **11** derivatives [28]. The TA spectra and kinetics of **1** and **2** are fairly similar (Fig. 3 and S2), confirming negligible differences in the photophysics of both compounds. Fig. S3A shows likewise a dominant ESA centered around 550 nm with a second ESA band at 375 nm. The transient decay at 550 nm of **2** in $CHCl_3$ reveals a time constant of 23 ps which matches well with that value obtained for **1**.

Fig. 4A and S4A display the TA spectra of **6** and **5** in toluene upon excitation at λ_{exc} = 387 nm, respectively. In both cases an ESA is detected with a maximum around 500 nm. The shift in ESA compared to the brominated molecules, **1** and **2**, is already a hint for a different energetic scheme. Fig. 4B and S4B show the time profiles at λ_{probe} = 500 nm for **6** and **5** indicating once more a fast excited state de-activation. As it was reported for **1**, the TA dynamics decay much faster when

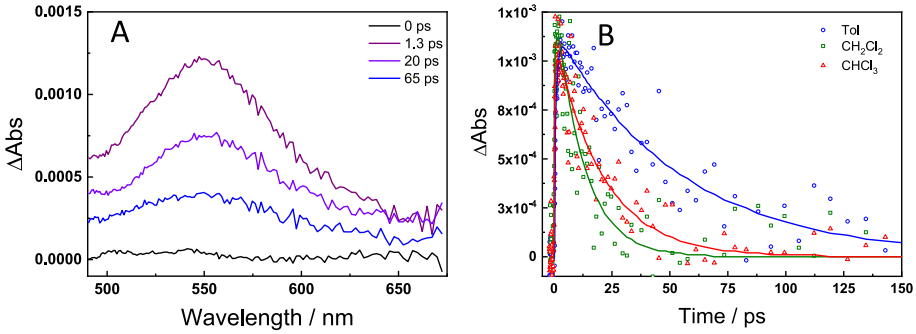

Fig. 3. (A) Transient absorption spectra of **1** at different time delays after photoexcitation at λ_{exc} = 387 nm. (B) Transient absorption dynamics of **1** at λ_{probe} = 550 nm for three different solvents: toluene (blue circles), CH_2Cl_2 (green squares) and $CHCl_3$ (red triangles). The solid lines represent the best exponential fit of the experimental data.

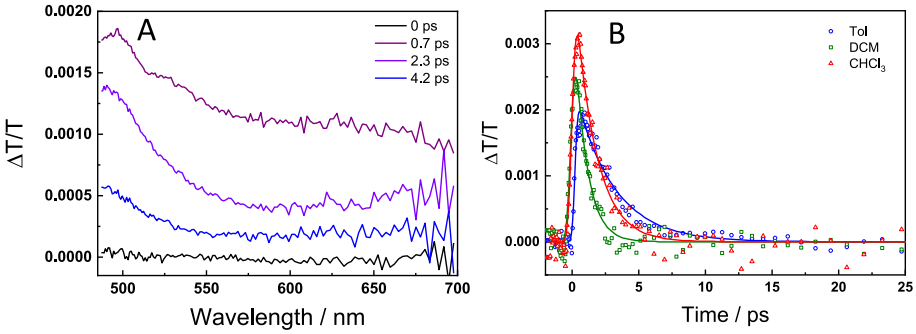

Fig. 4. (A) Transient absorption spectra of **6** at different time delays after photoexcitation at λ_{exc} = 375 nm. (B) Transient absorption dynamics of **6** at λ_{probe} = 500 nm for three different solvents, toluene (blue circles), CH_2Cl_2 (green squares) and $CHCl_3$ (red triangles). The solid lines represent the best exponential fit of the experimental data.

increasing the solvent polarity, for example 3.7, 1.66 and 1.08 ps for **5** in toluene, $CHCl_3$ and CH_2Cl_2, respectively.

This result strongly indicates that the same photophysical de-activation mechanism as in **1** and **2** operates in the **6** and **5** derivatives. However, the time constants obtained from a mono-exponential fit of the experimental data are much shorter in **6** and **5** compared to **1** and **2** (see Fig. 5). In fact, the fast de-activation kinetics in **6** and **5** are comparable to those observed in isoindigo [46] despite their structural similarity with the non-functionalized *N,N*-dialkyl diazaisoindigo **9**, **10** and **11** derivatives. Thus, the insertion of the thiophenyl groups into the diazaisoindigo platform favors the ultrafast non-radiative internal conversion process.

Regarding the mono substituted thiophenyl derivatives, **7** and **8**, Figs. S5 and S6 depict the TA spectra and TA dynamics of both molecules in $CHCl_3$. The transient spectra of **7** with only one thiophenyl group is identical to that of the other two di-substituted mono thiophenyl derivatives, **5** and **6**, with a ESA band in 400–700 nm visible region, and with maximum around 450 nm. However, the TA spectra for the dithiophenyl derivative, **8**, display a slightly different behaviour with ESA peaking around 650 nm and a negative signal in the ascribed 325–400 nm region. The latter transient feature may be assigned to the ground state bleach on account of spectral overlap with ground-state absorption. However, the TA dynamics for both mono-substituted derivatives, **7** and **8**, reveal similar time constants than for the di-substituted molecules. Fig. 5 display a comparative assessment of the TA dynamics and decay time constants for all molecules. On one side, the kinetics of **1** and **2** are similar to those of non-functionalized *N,N*-dialkyl diazaisoindigo **9**, **10** and **11** derivatives when comparing the decay time constants of our TA measurements with those previously reported for time-resolved fluorescence experiments [28]. On the other side, the kinetics of all thiophenyl **5**–**8** derivatives exhibit a much faster excited state deactivation which could be related to an increase of the non-radiative rate constant. The incorporation of thiophenyl groups could accelerate the non-radiative deactivation through a conical intersection point between S_1 and S_0 states (the common mechanism attributed to diazaisoindigo derivatives). In this regard, the relative energy of the LUMO orbital in the isoindigo based chromophores has been claimed to play a key role in the efficiency of the non-radiative de-activation [46,54]. Thus, the increase of the LUMO energy in the thiophenyl derivatives can be related to a lower value of the activation energy of the twisting process which might explain the faster excited state de-activation in this family of compounds. Additionally, the competition between different non-radiative deactivation mechanisms cannot be ruled out, as proposed for isoindigo derivatives [46].

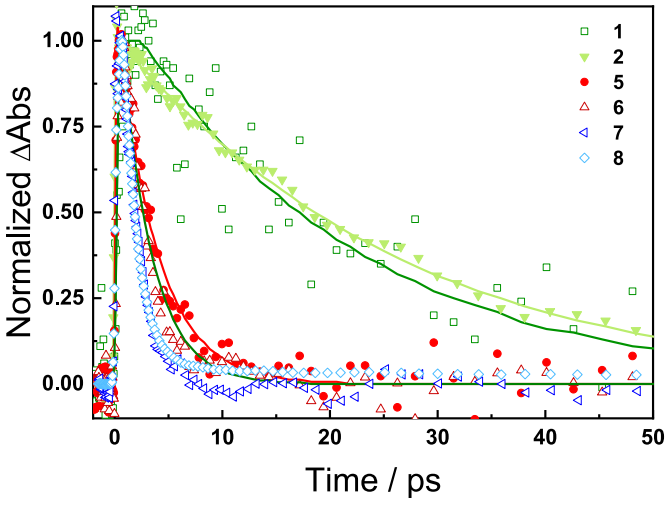

Fig. 5. Normalized transient absorption dynamics of **1** (green squares), **2** (green triangles), **5** (red circles), and **6** (red triangles), **7** (blue triangles) and **8** (blue diamonds) in toluene. Probe wavelengths were 550 nm (**1**,**2**) 500 nm (**5**,**6**), 450 nm (**7**) and 650 nm (**8**). The solid lines represent the best exponential fit of the experimental data.

4. Conclusion

In summary, we have developed different D-A-D and D-A conjugated triads and dyads of diazaisoindigos with thiophenyl derivatives in 5,5′- and 5- position of this platform. The incorporation of the electron-donor thiophenyl moiety in the diazaisoindigo does not lead to significant change of the molecular structure of the 7,7′-diazaisoindigo but the electronic structure is significantly altered. Important modifications were observed in the absorption spectra of **5**–**8** with respect to **1** and **2**, attributed to the change in the energy and localization of the frontier orbitals. Fluorescence emission was only observed for **1** and **2**, while the small oscillator strengths calculated for the $S_0 \rightarrow S_1$ transition of **5**–**8** suggested that the incorporation of thiophenyl groups leads to a decrease of the radiative rate constant. The picosecond TA experiments revealed shorter time decays for the thiophenyl derivatives also indicating a much faster excited state de-activation due to the twisting of the central double bond to reach a conical intersection between the excited and ground states.

CRediT authorship contribution statement

M. Belén Martin: Formal analysis, Investigation, Methodology. **Álvaro Recuero:** Formal analysis, Investigation, Methodology. **Andrés Garzón-Ruiz:** Formal analysis, Data curation, and, Supervision, Writing – review & editing. **Mónica Moral:** Formal analysis, Data curation, and, Supervision. **Gonzalo García-Espejo:** Formal analysis, Investigation, Methodology. **Juan Cabanillas-Gonzalez:** Data curation, Supervision, Funding acquisition, Methodology, Resources, Writing – original draft, Writing – review & editing. **Gustavo de Miguel:** Data curation,

Supervision, Funding acquisition, Methodology, Resources, Writing – original draft, Writing – review & editing. **Eva M. García-Frutos:** Conceptualization, Data curation, Supervision, Validation, Methodology, Resources, Funding acquisition, Writing – original draft, Writing – review & editing.

Declaration of competing interest

The authors declare that they have no known competing financial interests or personal relationships that could have appeared to influence the work reported in this paper.

Data availability

Data will be made available on request.

Acknowledgments

E.M.G.F acknowledges the Spanish Ministry of Science and Innovation MCIN/AEI/https://doi. org/10. 13039/50110 00110 33 [Spain, project PID2019-105479RB-I00]. G.M. gratefully acknowledges the financial Support for PID2020-119209RB-I00 project grant funded by MCIN/AEI/10.13039/501100011033 by "ERDF A way of making Europe". This research was also supported by Andalusian Government through PY20_01151 project funded by the EU through "Fondo Europeo de Desarollo Regional" (FEDER). J.C-G acknowledges support from the Spanish Ministry of Science and Innovation (RTI2018-097508−B-I00, CTQ2017-87054, PGC2018-096444-B-I00 and PID2021-128313OB-I00), the Regional Government of Madrid through projects NMAT2D-CM (S2018/NMT-4511), the program Proyectos Sinérgicos de I + D (Grant Y2018/NMT-5028 FULMATEN-CM), NANOCOV-CM (REACT-UE), and by the Campus of International Excellence (CEI) UAM + CSIC. IMDEA Nanociencia acknowledges support from the Severo Ochoa Programme for Centres of Excellence in R&D (MINECO, grant CEX2020-001039-S).

Appendix A. Supplementary data

Supplementary data to this article can be found online at https://doi.org/10.1016/j.dyepig.2023.111197.

References

[1] Zaumseil J, Sirringhaus H. Electron and ambipolar transport in organic field-effect transistors. Chem Rev 2007;107:1296–323. https://doi.org/10.1021/cr0501543.
[2] Guo X, Facchetti A J, Marks T. Imide- and amide-functionalized polymer semiconductors. Chem Rev 2014;114:8943–9021. https://doi.org/10.1021/cr500225d.
[3] Dou L, Liu Y, Hong Z, Li G, Yang Y. Low-bandgap near-IR conjugated polymers/molecules for organic electronics. Chem Rev 2015;115:12633–65. https://doi.org/10.1021/acs.chemrev.5b00165.
[4] Wang C, Zhang X, Dong H, Chen X, Hu W. Challenges and emerging opportunities in high-mobility and low-energy-consumption organic field-effect transistors. Adv Energy Mater 2020;10:2000955. https://doi.org/10.1002/aenm.202000955.
[5] Wang C, Dong H, Hu W, Liu Y, Zhu D. Semiconducting π - conjugated systems in field-effect transistors: a material odyssey of organic electronics. Chem Rev 2011;112:2208–67. https://doi.org/10.1021/cr100380z.
[6] Grolleau J, Gohier F, Allain M, Legoupy S, Cabanetos C, Frère P. Rapid and green synthesis of complementary D-A small molecules for organic photovoltaics. Org Electron 2017;42:322–8. https://doi.org/10.1016/j.orgel.2016.12.046.
[7] Fabara AN, Fraaije MW. An overview of microbial indigo-forming enzymes. Appl Microbiol Biotechnol 2020;104:925–33. https://doi.org/10.1007/s00253-019-10292-5.
[8] Kim T-D, Lee K-S D-π-A. Conjugated molecules for optoelectronic applications. Macromol Rapid Commun 2015;36:943–58. https://doi.org/10.1002/marc.201400749.
[9] Yao H, Cui Y, Yu R, Gao B, Zhang H, Hou J. Design, synthesis, and photovoltaic characterization of a small molecular acceptor with an ultra-narrow band gap. Angew Chem 2017;129:3091–5. https://doi.org/10.1002/ange.201610944.
[10] Zhang J, Xu W, Sheng P, Zhao G, Zhu D. Organic donor–acceptor complexes as novel organic semiconductors. Accounts Chem Res 2017;50:1654–62.
[11] Zhang M, Nok Tsao H, Pisula W, Yang C, Mishra A K, Müllen K. Field-effect transistors based on a Benzothiadiazole-Cyclopentadithiophene copolymer. J Am Chem Soc 2007;129:3472–3. https://doi.org/10.1021/ja0683537.
[12] Gautam P, Maragania R, Misra R. Aryl-substituted symmetrical and unsymmetrical benzothiadiazoles. RSC Adv 2015;5:18288–94. https://doi.org/10.1039/C4RA15424J.
[13] Li W S, Christian Roelofs W, Wienk M M, Janssen R AJ. Enhancing the photocurrent in diketopyrrolopyrrole-based polymer solar cells via energy level control. J Am Chem Soc 2012;134:13787–95. https://doi.org/10.1021/ja305358z.
[14] Seung Ha J, Hwan Kim K, Hoon Choi D. 2,5-Bis(2-octyldodecyl)pyrrolo[3,4-c]pyrrole-1,4-(2H,5H)-dione-Based donor–acceptor alternating copolymer bearing 5,5'-Di(thiophen-2-yl)-2,2'-biselenophene exhibiting 1.5 $cm^2 \cdot V^{-1} \cdot s^{-1}$ hole mobility in thin-film transistors. J Am Chem Soc 2011;133:10364–7. https://doi.org/10.1021/ja203189h.
[15] Patil Y, Popli C, Misra R. Near-infrared absorbing tetracyanobutadiene-bridged diketopyrrolopyrroles. New J Chem 2018;42:3892–9. https://doi.org/10.1039/C7NJ05162J.
[16] Lei T, Dou J-H, Cao X-Y, Wang J-Y, Pei J. Electron-deficient poly(p-phenylene vinylene) provides electron mobility over 1 $cm^2\ V^{-1}\ s^{-1}$ under ambient conditions. J Am Chem Soc 2013;135:12168–71. https://doi.org/10.1021/ja403624a.
[17] Lei T, Wang J-Y, Pei J. Design, synthesis, and structure–property relationships of isoindigo-based conjugated polymers. Acc Chem Res 2014;47:1117–26. https://doi.org/10.1021/ar400254j.
[18] Stalder R, Mei J, Graham KR, Estrada LA, Reynolds JR. Isoindigo, a versatile electron-deficient unit for high-performance organic electronics. Chem Mater 2014;26:664–78. https://doi.org/10.1021/cm402219v.
[19] Fallon K J, Wijeyasinghe N FManley E, Dimitrov S D, Yousaf S A, Ashraf R S, et al. Indolo-naphthyridine-6,13-dione thiophene building block for conjugated polymer electronics: molecular origin of ultrahigh n-type mobility. Chem Mater 2016;28:8366–78. https://doi.org/10.1021/acs.chemmater.6b03671.
[20] Rout Y, Chauhan V, Misra R. Synthesis and characterization of isoindigo-based push–pull chromophores. J Org Chem 2020;85(7):4611–8. https://doi.org/10.1021/acs.joc.9b03267.
[21] Maugard T, Enaud E, Choisy P, Legoy MD. Identification of an indigo precursor from leaves of Isatis tinctoria (Woad). Phytochemistry 2001;58:897–904. https://doi.org/10.1016/S0031-9422(01)00335-1.
[22] Stalder R, Mei J, Graham K R, Estrada L A, Isoindigo R Reynolds J. A versatile electron-deficient unit for high-performance organic electronics. Chem Mater 2013;26:664–78. https://doi.org/10.1021/cm402219v.
[23] Mei J R, Graham K, Stalder R, Reynolds J R. Synthesis of isoindigo-based oligothiophenes for molecular bulk heterojunction solar cells. Org Lett 2010;12:660–3. https://doi.org/10.1021/ol902512x.
[24] Wang E, Mammo W, Andersson MR. 25th anniversary article: isoindigo-based polymers and small molecules for bulk heterojunction solar cells and field effect transistors. Adv Mater 2014;26:1801–26. https://doi.org/10.1002/adma.201304945.
[25] Liang L, Chen X-Q, Xiang X, Ling J, Shao W, Lu Z, et al. Searching proper oligothiophene segment as centre donor moiety for isoindigo-based small molecular photovoltaic materials. Org Electron 2017;42:93–101. https://doi.org/10.1016/j.orgel.2016.12.028.
[26] Li J-L, Cao J-J, Duan L-L, Zhang H-L. Evolution of isoindigo-based electron-deficient units for organic electronics: from natural dyes to organic semiconductors. Asian J Org Chem 2018;7:2147–60. https://doi.org/10.1002/ajoc.201800198.
[27] Randell NM, Kelly TL. Recent advances in isoindigo-inspired organic semiconductors. Chem Rec 2019;19:973–88. https://doi.org/10.1002/tcr.201800135.
[28] de Miguel G, Camacho L, García-Frutos EM. 7,7'-Diazaisoindigo: a novel building block for organic electronics. J Mater Chem C 2016;4:1208–14. https://doi.org/10.1039/C5TC03464G.
[29] Moral M, Navarro A, Garzón-Ruiz A, García-Frutos E M. Tuning the crystal packing and semiconductor electronic properties of 7,7'-diazaisoindigo by side-chain length and halogenation. J Phys Chem C 2018;123:153–64. https://doi.org/10.1021/acs.jpcc.8b09633.
[30] Garzón A, Navarro A, López D, Perles J, García-Frutos E M. Aggregation-induced enhanced emission (AIEE) from *N,N*-Octyl-7,7'-diazaisoindigo-Based organogel. J Phys Chem C 2017;121:27071–81. https://doi.org/10.1021/acs.jpcc.7b07625.
[31] Huang J, Mao Z, Chen Z, Gao D, Wei C, Zhang W, et al. Diazaisoindigo-based polymers with high-performance charge-transport properties: from computational screening to experimental characterization. Chem Mater 2016;28:2209–18. https://doi.org/10.1021/acs.chemmater.6b00154.
[32] Lu Y, Liu Y, Dai Y-Z, Yang C-Y, Un H-I, Liu S-W, et al. 5,5'-Diazaisoindigo: an electron-deficient building block for donor–acceptor conjugated polymers. Chem Asian J 2017;12:302–7. https://doi.org/10.1002/asia.201601671.
[33] Ashizawa M, Hasegawa T, Kawauchi S, Masunaga H, Hikima T, Sato H, et al. Influence of structure–property relationships of two structural isomers of thiophene-flanked diazaisoindigo on carrier-transport properties. RSC Adv 2016;6:109434–41. https://doi.org/10.1039/C6RA17424H.
[34] Huang K, Zhao X, Du Y, Kim S, Wang X, Lu H, et al. Modulating charge transport characteristics of bis-azaisoindigo-based D–A conjugated polymers through energy level regulation and side chain optimization. J Mater Chem C 2019;7:7618–26. https://doi.org/10.1039/C9TC02021G.
[35] Yue W, Li C, Tian X, Li W, Neophytou M, Chen H, et al. Diazaisoindigo bithiophene and terthiophene copolymers for application in field-effect transistors and solar cells. J Polym Sci Part A Polym Chem 2017;55:2691–9. https://doi.org/10.1002/pola.28676.
[36] Li D, Wang X, Lin Z, Zheng Y, Jiang Q, Zheng N, et al. Tuning charge carrier and spin transport properties via structural modification of polymer semiconductors.

ACS Appl Mater Interfaces 2019;11:30089–97. https://doi.org/10.1021/acsami.9b07863.
[37] Frisch MJ, Trucks GW, Schlegel HB, Scuseria GE, Robb MA, Cheeseman JR, et al. Gaussian 16, revision C.01. 2016.
[38] Perdew JP, Burke K, Ernzerhof M. Generalized gradient approximation made simple. Phys Rev Lett 1996;77:3865–8. https://doi.org/10.1103/PhysRevLett.77.3865.
[39] Adamo C, Barone V. A TDDFT study of the electronic spectrum of s-tetrazine in the gas-phase and in aqueous solution. Chem Phys Lett 2000;330:152–60. https://doi.org/10.1016/S0009-2614(00)01082-4.
[40] Cossi M, Rega N, Scalmani G, Barone V. Energies, structures, and electronic properties of molecules in solution with the C-PCM solvation Model. J Comput Chem 2003;24:669–81. https://doi.org/10.1002/jcc.10189.
[41] Tomasi J, Mennucci B, Cammi R. Quantum mechanical continuum solvation models. Chem Rev 2005;105:2999–3094. https://doi.org/10.1021/cr9904009.
[42] Guido CA, Cortona P, Mennucci B, Adamo C. On the metric of charge transfer molecular excitations: a simple chemical descriptor. J Chem Theor Comput 2013;9:3118–26. https://doi.org/10.1021/ct400337e.
[43] Lu T, Chen F. Multiwfn: a multifunctional wavefunction analyzer. J Comput Chem 2012;33. https://doi.org/10.1002/jcc.22885.
[44] Cheng X, Merz K-H, Vatter S, Christ J, Wölfl S, Eisenbrand G. 7,7`-Diazaindirubin—a small molecule inhibitor of casein kinase 2 in vitro and in cells. Bioorg Med Chem 2014;22:247–55. https://doi.org/10.1016/j.bmc.2013.11.031.
[45] Batsanov SS. Van der Waals radii of elements. Inorg Mater 2001;37:871–85. https://doi.org/10.1023/A:1011625728803.
[46] Estrada LA, Stalder R, Abboud KA, Risko C, Brédas JL, Reynolds JR. Understanding the electronic structure of isoindigo in conjugated systems: a combined theoretical and experimental approach. Macromolecules 2013;46:8832–44. https://doi.org/10.1021/ma4013829.
[47] Strickler SJ, Berg RA. Relationship between absorption intensity and fluorescence lifetime of molecules. J Chem Phys 1962;37:814–21. https://doi.org/10.1063/1.1733166.
[48] Vikesland JP, Strickler SJ. $^3B_1$-$^1A_1$ transition of SO_2 gas. I. Franck-Condon treatment and transition moments. J Chem Phys 1974;60:660–3. https://doi.org/10.1063/1.1681089.
[49] Moral M, Tolosa J, Canales-Vázquez J, Carlos Sancho-García J, Garzón-Ruiz A, García-Martínez JC. Combined theoretical and experimental study on intramolecular charge transfer processes in star-shaped conjugated molecules. J Phys Chem C 2019;123:11179–88. https://doi.org/10.1021/acs.jpcc.8b12248.
[50] Pacheco-Liñán PJ, Navarro A, Tolosa J, Moral M, Martín C, Bravo I, Hofkens J, García-Martínez JC, Garzón-Ruiz A. Intramolecular charge transfer and molecular flexibility: key parameters to be considered in the design of highly fluorescent p-phenylene vinylene derivatives. Dyes Pigments 2022;199:110105. https://doi.org/10.1016/j.dyepig.2022.110105.
[51] Panchenko PA, Arkhipova AN, Zakharko MA, Jonusauskas G, Fedorov YV, Fedorova OA. Synthesis and spectral properties of fluorescent dyes based on 4-styryl-1,8-naphthalimide. Russ Chem Bull 2016;65:2444–51. https://doi.org/10.1007/s11172-016-1604-8.
[52] Thorat KG, Ray AK, Sekar N. Modulating TICT to ICT characteristics of acid switchable red emitting boradiazaindacene chromophores: perspectives from synthesis, photophysical, hyperpolarizability and TD-DFT studies. Dyes Pigments 2017;136:321–34. https://doi.org/10.1016/j.dyepig.2016.08.049.
[53] Quenneville J, Martínez TJ. Ab initio study of Cis-Trans photoisomerization in stilbene and ethylene. J Phys Chem A 2003;107:829–37. https://doi.org/10.1021/jp021210w.
[54] Perpète EA, Preat J, André J-M, Jacquemin D. An ab initio study of the absorption spectra of indirubin, isoindigo, and related derivatives. J Phys Chem A 2006;110:5629–35. https://doi.org/10.1021/jp060069e.